energies

MDPI

Article

Latent Thermal Energy Storage for Cooling Demands in Battery Electric Vehicles: Development of a Dimensionless Model for the Identification of Effective Heat-Transferring Structures

Volker Dreißigacker * and Andrea Gutierrez

Institute of Engineering Thermodynamics, German Aerospace Center, Pfaffenwaldring 38–40, 70569 Stuttgart, Germany; andrea.gutierrezrojas@dlr.de
* Correspondence: volker.dreissigacker@dlr.de

Abstract: Thermal energy storage (TES) systems open up alternative paths for air conditioning to increase the range of battery electric vehicles (BEVs) by reducing power consumption. The central prerequisites for this purpose are high storage densities: high-temperature TES systems are being focused on for heat demands, while effective solutions for cooling are missing. Due to their lower temperature potentials, concepts with high storage capacities and heat transports between the storage and cold transferring medium are needed. Latent TES systems based on water enable these capacities but require adequate internal structures for effective heat transfer. Due to the large number of geometric options, high simulation efforts must be conducted to identify favored structures, or the possible design space must be limited for investigations. For this purpose and for the first time, an alternative way is presented using newly developed dimensionless models in a top-down methodology for time-efficient design studies and evaluations. These models were successfully validated and used as a design tool to identify effective structures in latent TES systems for cooling demands in BEVs. A wide array of variation studies on tube, finned plate and novel Triply Periodic Minimal Surface (TPMS) structures were performed and uniformly evaluated with regard to storage densities, cooling efficiencies and geometry. The results show high storage densities for novel TPMS structures, including the enclosure of 100 Wh/kg or 102.2 kWh/m^3 with average cooling capacities of 1 kW over 30 min, confirming the usability of latent TES systems in terms of compactness and efficiency for cooling demands in BEVs.

Keywords: latent thermal energy storage; dimensionless model; battery electric vehicle; triply periodic minimal surface

Citation: Dreißigacker, V.; Gutierrez, A. Latent Thermal Energy Storage for Cooling Demands in Battery Electric Vehicles: Development of a Dimensionless Model for the Identification of Effective Heat-Transferring Structures. *Energies* **2024**, *17*, 6218. https://doi.org/10.3390/en17246218

Academic Editor: Enrique Romero-Cadaval

Received: 19 November 2024
Revised: 3 December 2024
Accepted: 5 December 2024
Published: 10 December 2024

1. Introduction

The expansion of renewable energies requires increasingly flexible options for different power and time scales to efficiently balance fluctuating (electrical) energy generation and consumption. Energy storage technologies are ideal solutions for stationary applications, as their time-decoupled operation creates a buffer between supply and demand. In addition to batteries, thermal energy storage (TES) systems are particularly suitable for large-scale applications: as central elements within thermodynamic cycles [1–3], they form the basis for cyclical storage operation or improved operational flexibility. In addition, these options open up sector coupling, for example through waste heat utilization and upgrading [4], or additional operational flexibility and cost reduction potential through power-to-heat expansions [5].

Integration concepts for TES in electrically powered vehicles are also being investigated, and they enable alternative air conditioning options and, thus, increased range through reduced battery consumption [6]. In contrast to stationary applications, solutions are required that reach high storage and power densities to fulfil space requirements. In

the case of hydrogen-electric vehicles, thermochemical storage systems are being considered [7,8], which provide heat and cold through a reversible reaction path. For battery electric vehicles (BEVs), investigations are being conducted onto solid-medium [9] and metallic-latent TES systems [10,11], which are heated electrically to high temperatures of over 600 °C before driving (charging) and allow a heat supply at a constant temperature level in the range of 20 to 60 °C via a bypass system during driving (discharging). High storage densities of 150 Wh/kg and constant thermal powers of over 5 kW have already been experimentally confirmed, particularly for solid-medium storage systems [12]. However, the scope of these options has so far focused on heat during cold seasons; efficient solutions for cooling requirements in warm seasons are still missing.

When using TES systems to supply BEVs with cooling, the low temperature difference poses significantly greater challenges in terms of storage density. For example, in today's vehicles, typical compression refrigeration systems' minimal operating temperatures between −10 and −30 °C are reached, which represent a lower limit for charging a systemic integrated storage unit. Peltier elements, as an alternative cooling option, allow temperature differences of up to 70 K, leading to similar cooling ranges and thus to comparable challenges in terms of storage density. Regardless of the existing cooling source and integration options, the low temperature potential presents a major hurdle for compact TES systems. To overcome such limitations, two central requirements are necessary: high (material) specific storage capacities and effective heat transport between the storage and the cold transporting medium. The former requirement can be met by latent TES [13] using suitable phase change materials (PCMs) and utilizing the fusion enthalpy; the latter can be met by selecting a suitable internal heat-transferring structure.

In relation to the boundary conditions in BEVs, water is the favored solution due to its high fusion enthalpy, suitable melting temperature and cost-effective and risk-free handling. In addition to water, alternative materials with melting temperatures of up to −50 °C were also investigated for mobile applications and are summarized in [14,15]. A significantly greater number of potential degrees of freedom is available when selecting a suitable heat-transferring structure that separates the PCMs from the (sensible) fluid medium. Regardless of the application, two basic options have been widely considered for this purpose: tube [16] and finned plate systems [17]. In addition, there has been an increasing number of publications for some years investigating TPMS-based geometries (Triply Periodic Minimal Surface) for heat exchangers [18,19] or as heat-conducting structures within a PCM [20,21] for battery thermal management. Together with the established structures, this results in a multitude of geometric options for heat-transferring surfaces inside latent TES systems, each associated with high efforts in conceptual and simulative design. Today, latent storage models use either complex CFD-based simulations [16,17,20,21] for selected structures or approximation functions including simplifications to capture the radial progression of the melting front at constant cooling temperatures [22–24], whereby axial effects during heat transport—especially in applications with a sensible fluid—are not considered. Alternative methods are therefore being sought for the identification of efficient latent TES solutions for cooling demands in BEVs.

For this purpose and for the first time, a top-down approach based on a dimensionless (axial) model for latent TES systems is presented. With this tool, dimensionless solutions are derived fulfilling the defined target values, whereby their model parameters form the basis for direct design evaluations. The enthalpy and temperature-based, dimensionless (axial) model for PCMs and sensible fluids allows for investigations of relevant transient characteristics and a computational efficient derivation of geometry-specific design solutions via its model parameters. The model derivation is based on geometric equivalence values (specific surface and void fraction), normalization and relation procedures, as well as on a novel dimensionless parameterization of the thermal conduction resistance inside the PCM, combining the theoretical approaches of regenerators [25,26] and latent TES systems [27]. With this universal tool, it is now possible to identify effective structures

from a large number of geometric options, which form the basis in further design works for subsequent detailed analyses.

The overall aim of this publication is divided into two parts: firstly, to develop a new dimensionless model for latent TES with sensible fluids as heat/cold transferring media including a parametrization of the thermal conduction resistance in the phase change material; secondly, to use this model for the first time in a top-down methodology for the identification of effective structures in latent TES for high storage densities. The development of the dimensionless models, including verification and validation, and their use for identifying effective structures in latent TES systems, is presented below. Herein, in addition to well-known tube and finned plate systems, novel TPMS structures are considered as a further geometric option.

2. Triply Periodic Minimal Surface (TPMS) Geometries

For the identification of efficient heat-transferring structures, geometry configurations are investigated on the base of tube and finned plate systems and TPMS options. These novel geometries belong to a class of lattice structures, whose shape is described by trigonometric functions and which are constructed via 3D-printing processes. The resulting geometries consist of two periodically arranged, interwoven channels that are separated from each other by a wall. Depending on the TPMS option, the cyclically repeating structures differ, whereby the respective shape can be modified by their equation parameters. Typical variants analyzed in the literature in the context of Nusselt and pressure loss correlations are known as Gyroid, Schwarz-D, Schwarz-P, Neovius, Schoen's I-WP and Fischer-Koch S [28,29]. Due to their high heat transfer coefficients and simultaneously high specific surfaces, such structures are suitable geometric configurations in latent TES systems. An overview of well-known TPMS geometries is summarized in Figure 1.

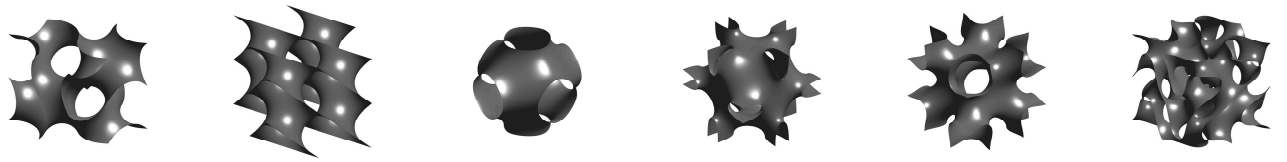

(**a**) Gyroid (**b**) Schwarz-D (**c**) Schwarz-P (**d**) Neovius (**e**) Schoen's I-WP (**f**) Fischer-Koch S

Figure 1. TPMS (Triply Periodic Minimal Surface) design options.

The investigations performed here include a Fischer-Koch S structure as an exemplary TPMS option in addition to the tube and finned plate systems. Compared to the alternative TPMS structures, this option is characterized in particular by high heat transfer and a specific surface. All considered geometry configurations are based on alternating channels of PCM storage and cold transferring medium.

In the context of this application, the selected structures form the basis for identifying efficient latent TES systems with high storage densities for supplying cold in BEVs. However, the presented dimensionless model in the following section is suitable as a universal tool, independent of the structures and application investigated herein.

3. Modeling

The developed model for latent TES is based on an axial formulation for the storage and fluid medium, whereby the conduction resistance within the PCM is considered in an effective heat transfer coefficient. The central aspects for both the dimensionless axial model and a parameterization of the thermal resistance are presented below.

3.1. Dimensionless Axial Model

The dimensionless model for latent TES is based on the (heterogeneous) approach for regenerators developed by Schumann [30], which divides the space into a storage (S) and fluid medium (F) and couples the heat transport between both via a geometric equivalence

value—specific surface (a_W)—and a heat transfer coefficient ($\bar{k}$). Here, dashes over values represent radially averaged quantities, whose derivation will be found in Section 3.2.

Expressed in terms of enthalpies (h), the originally temperature-based (T) transient (t) formulation of the storage medium is shown Equation (1).

$$(1-\Psi)\rho_S \frac{\partial \overline{h}_S}{\partial t} = \overline{k} a_W \left(T_F - \overline{T}_S\right) \tag{1}$$

The variable ρ represents the density and the expression (1 – Ψ)—as a further geometric equivalence value—represents the volume fraction (V) of the PCM within the space including the heat-transferring wall (W) according to Equation (2).

$$(1-\Psi) = \frac{V_S}{V_S + V_F + V_W} \tag{2}$$

The fluid is regarded as a sensible medium described by the original temperature-based (T) formulation. By neglecting the fluid-side storage term and heat losses, the axial (x) expression is obtained according to Equation (3):

$$\epsilon \rho_F c_F w_F \frac{\partial T_F}{\partial x} = \overline{k} a_W \left(\overline{T}_S - T_F\right) \tag{3}$$

where c and w represent the specific storage capacity and flow velocity for charging or discharging and ε the volume fraction of the fluid medium within the space as given in Equation (4).

$$\epsilon = \frac{V_F}{V_S + V_F + V_W} \tag{4}$$

Using theoretical approaches for regenerators [25,26] and latent TES systems [27], a dimensionless model is derived from Equations (1)–(4) by temporal (ξ) and axial normalizations (η_x) via the period τ and length L according to Equations (5) and (6):

$$\xi = \frac{t}{\tau} \tag{5}$$

$$\eta_x = \frac{x}{L} \tag{6}$$

and by relations to the melting enthalpy $\Delta h_{S,0}$ and temperature $T_{S,0}$ according to Equations (7) and (8):

$$\overline{z}_S = \frac{\overline{h}_S}{\Delta h_{S,0}} \tag{7}$$

$$y_i = \frac{T_i}{T_{S,0}} \tag{8}$$

resulting in the following formulations for the storage and fluid medium as described in Equations (9) and (10):

$$\frac{\partial \overline{z}_S}{\partial \xi} = \Pi(y_F - \overline{y}_S) \tag{9}$$

$$\frac{\partial y_F}{\partial \eta_x} = \Lambda(\overline{y}_S - y_F) \tag{10}$$

The state variables $\bar{z}$ und y represent the de-dimensionalized enthalpy and temperature. For the PCM, the relationship between enthalpy and temperature can be determined via the fusion enthalpy, melting temperature and specific heat capacities for the solid or liquid phase.

The design and material-specific parameters for the latent TES system are summarized in the resulting dimensionless parameters Π and Λ and shown in Equations (11) and (12):

$$\Pi = \frac{\bar{k} a_W V \tau T_{S,0}}{\Delta h_{S,0} m_S} \tag{11}$$

$$\Lambda = \frac{\bar{k} a_W V}{\dot{m}_F c_F} \tag{12}$$

where the quantity $\dot{m}_F$ represents the mass flow rate of the sensible fluid medium; m_S and V are the PCM storage mass and the total volume of the containment.

The formulations of the latent TES system according to Equations (9) and (10) illustrate that only two parameters and the relationship between enthalpy and temperature for the PCM are necessary for transient investigations in the axial direction. Thereby, the effective heat transfer coefficient ($\bar{k}$) within both parameters is the central value, whose magnitude is decisive for the storage characteristic. In addition to the convective heat transfer, this includes the thermal conduction resistances in the heat-transferring wall and PCM and thus represents the total heat transport transverse to the axial direction.

A detailed description of the effective heat transfer coefficient as a function of central influencing values is necessary in order to enable well-founded design studies. The central modeling aspects are presented in the following section.

3.2. Parametrization of Effective Heat Transfer Coefficient ($\bar{k}$)

The effective heat transfer coefficient ($\bar{k}$) within the dimensionless parameters Π and Λ covers, in a compact way, the total heat transport between the fluid and storage medium. For its dimensionless parameterization, a cylindrical substitute model is used, which captures the local heat transfer inside the PCM including the heat-transferring wall.

3.2.1. Dimensionless Radial Substitute Model

A cylindrical (radial) approach is used as the base of the substitute model for the dimensionless parameterization of the effective heat transfer coefficient ($\bar{k}$). The methodology is based on the idea that an arbitrary structure can be transferred to equivalent geometries in terms of the hydraulic diameter and void fraction. Such geometric equivalent values are well known and often used in Nusselt correlations when determining heat transfer coefficients or thermal resistances, and even in pressure loss correlations.

The central geometry values required for the (radially) substitute model are shown schematically in Figure 2.

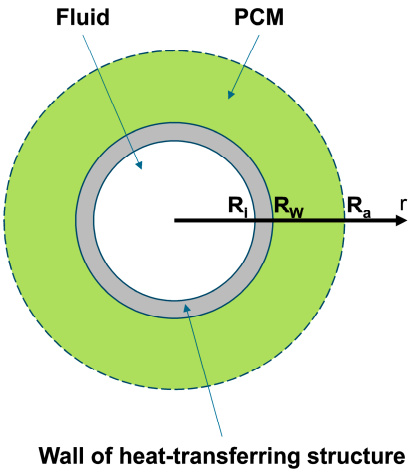

Figure 2. Substitute model with central geometric (equivalent) quantities: hydraulic radii at the outside of the fluid medium (R_i), outside of the wall (R_W) and outside of the PCM (R_a).

Here, the radial (r) and transient substitute model includes the PCM only as a capacity term. In principle, this assumption underestimates the total available storage capacity, but the capacitive proportion of the non-considered sensible wall is, compared to the PCM, negligible or very low, both in relation to mass and specific storage capacity. This well-founded simplification results in an enthalpy-based radial formulation according to Equation (13):

$$\rho_S \frac{\partial h_S}{\partial t} = \lambda_S \left[\frac{\partial^2 h_S}{\partial r^2} + \frac{1}{r} \frac{\partial h_S}{\partial r} \right] \tag{13}$$

where λ represents the radial heat conduction of the PCM.

For the dimensionless formulation, a radial normalization (η_r) according to Figure 2 is conducted as given in Equation (14):

$$\eta_r = \frac{r - R_W}{R_a - R_W} \tag{14}$$

which results together with Equations (5), (7) and (8) in the following expression for the storage medium (S) (15):

$$\frac{\partial z_S}{\partial \xi} = Fo\left(1 - \sqrt{\psi}\right)^{-2} \left[\frac{\partial^2 y_S}{\partial \eta_r^2} + \left(\eta_r + \frac{\sqrt{\psi}}{1 - \sqrt{\psi}} \right)^{-1} \frac{\partial y_S}{\partial \eta_r} \right] \tag{15}$$

Here, $1 - \Psi$ represents the already-known volume fraction of the PCM determined for the substitute model according to Equation (16):

$$\psi = \frac{R_W^2}{R_a^2} \tag{16}$$

and Fo represents the Fourier number as given in Equation (17).

$$Fo = \frac{\lambda_S T_{S,0} \tau}{\rho_S \Delta h_{S,0} R_a^2} \tag{17}$$

For a complete formulation of the radial heat transport, boundary conditions must be defined on the inside and outside of the model. Analogous to the described normalization and relation procedures, the convective boundary condition on the inside (η_r = 0) is expressed in a dimensionless formulation in Equation (18):

$$\frac{\partial y_S}{\partial \eta_r}|_{\eta_r=0} = Bi^* \left(1 - \sqrt{\psi}\right) [y_F(\eta_r = 0) - y_S] \tag{18}$$

and on the outside (η_r = 1) for an adiabatic boundary condition in Equation (19).

$$\frac{\partial y_S}{\partial \eta_r}|_{\eta_r=1} = 0 \tag{19}$$

Here, the dimensionless parameter Bi* represents the effective Biot number according to Equation (20):

$$Bi^* = \frac{\alpha^* R_a}{\lambda_S} \tag{20}$$

whereby the geometry-specific parameter α^* considers the heat transfer coefficient of the fluid α and the thermal resistance coefficient of the wall α_W as given in Equation (21).

$$\frac{1}{\alpha^*} = \frac{1}{\alpha} + \frac{1}{\alpha_W} \tag{21}$$

Using the dimensionless Equations (15), (18) and (19), transient and local temperature profiles can be determined as a function of the parameters *Fo*, *Bi** and Ψ. With variation studies on these, a dimensionless parameterization of the effective heat transfer coefficient ($\bar{k}$) can be performed. The model-based methodology for this is presented in the following section.

3.2.2. Dimensionless Effective 0D Model

The effective heat transfer coefficient ($\bar{k}$) is parameterized using results from the dimensionless equivalent model created in Section 3.2.1 and a 0D-based formulation of the heat transfer between the fluid (*F*) and the storage medium (*S*) according to Equation (22):

$$m_S \frac{\partial \bar{h}_S}{\partial t} = \bar{k} A_W \left(T_F - \overline{T}_S \right) \tag{22}$$

where A_W represents the heat-transferring surface of the wall.

Analogous to the normalization and relation procedures explained so far and using the relationship formulated in Equation (23), the original expression can be converted into a dimensionless Equation (24).

$$\frac{\bar{k}}{\alpha^*} = \frac{1}{1 + Bi^* \phi} \tag{23}$$

$$\frac{\partial \bar{z}_S}{\partial \xi} = 2 \frac{\sqrt{\psi}}{1 - \psi} Fo \frac{Bi^*}{1 + Bi^* \phi} (y_F - \bar{y}_S) \tag{24}$$

In addition to the already-known parameters (*Fo*, *Bi**, Ψ), a further parameter (ϕ) is introduced here, which is to be understood as a temporally averaged correction factor and which captures the effective conduction resistance within the PCM in the 0D-based model in comparison to the radially solved equivalent model. Therefore, results from the detailed (radial) equivalent model are required.

For this purpose, the resulting radial (η_r) and temporal (ξ) profiles of the state variable z_s = f (η_r,ξ) according to Equation (15) are used to calculate spatially integrated averaged values as expressed in Equation (25):

$$\bar{z}_{S,1D}(\xi) = \int_{\eta_r=0}^{\eta_r=1} z_S(\eta_r, \xi) \tag{25}$$

which serve as transient target values for the iterative adjustment of the correction factor ϕ in the 0D-based model as given in Equation (24). The correction factor is determined by minimizing the relative deviations according to Equation (26).

$$error(\phi) = \sum \left| \frac{\bar{z}_{S,1D}(\xi) - \bar{z}_S(\xi, \phi)}{\bar{z}_{S,1D}(\xi)} \right| \tag{26}$$

Based on this methodology and depending on the parameters (*Fo*, *Bi**, Ψ), the correction factor and thus the effective heat transfer coefficient ($\bar{k}$) is parameterized in Equation (23). The results of this, verifications and validations, and design calculations of latent TES systems for the cooling supply of BEVs are presented below.

4. Results

At the beginning of Section 4, results for the parametrization of the correction factor (ϕ) are presented according to the model details in Section 3.2. In the second step, the fully described, dimensionless axial model as given in Section 3.1 is verified and validated using published data on a tube and plate geometry. Finally, the successfully validated model is used for design studies to identify efficient structures in latent TES systems for the cooling supply of BEVs.

Therefore, the central model equations were discretized spatially with a resolution of 200 nodes and a constant mesh size using finite difference methods, both for the axial model

as given in Equations (9) and (10) as well as in the radial substitute model according to Equation (15). The resulting differential-algebraic systems of equations were then solved in time in Matlab R2020a (ode-solver) to determine the radial and axial profiles of the transient state variables. Temperature-averaged material data were used for the respective PCM and cold transport medium, whereby separate specific heat capacities were considered for the liquid and solid phases of the storage medium.

4.1. Parametrization of the Effective Heat Transfer Coefficient ($\bar{k}$)

For parametrization of the correction factor (ϕ) and, thus, the effective heat transfer coefficient ($\bar{k}$), variation studies were conducted for the dimensionless parameters (*Fo*, *Bi** and Ψ). The investigations cover a wide range of configurations and are summarized in Table 1.

Table 1. Variation ranges for parametrization of the correction factor *d*.

Fo	***Bi****	**Ψ**
0.01–1000	0.01–100	0.05–0.95

Processed results for the correction factor are shown in Figure 3. As already mentioned, the correction factor is to be understood as a temporally averaged value for the heat transport inside the PCM and thus as an effective thermal conduction resistance.

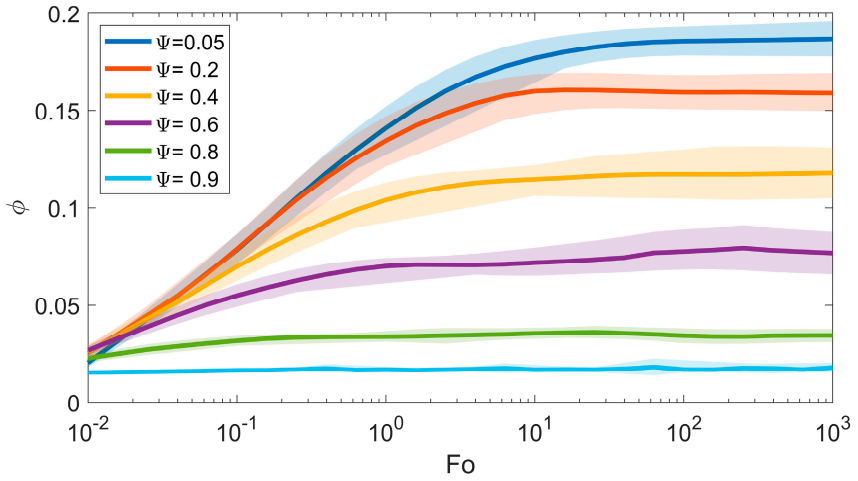

Figure 3. Correction factor (ϕ) as a function of Fourier number (*Fo*). The volume fraction of PCM ($1 - \Psi$) and the effective Biot number (*Bi**) are illustrated by hatched areas.

The correction factor (ϕ) tends asymptotically towards a maximum value, with an increasing Fourier number (*Fo*) depending on the volume fraction of the PCM (1 – Ψ). This behavior is due to the fact that higher thermal resistances effectively occur in the storage medium with increasing PCM proportions, but these are limited with increasing dimensionless duration (*Fo*) through lower spatially averaged temperature differences during transient heat transport. However, at low Fourier numbers the correction factor (ϕ) tends towards zero. With these associated low dimensionless durations, no significant changes in temperature in the PCM occur, resulting in a negligible influence on the transient heat transport and thus in the effective thermal resistance.

In contrast, the effective Biot number (*Bi**)—illustrated by the hatched areas—shows only slightly effects on the correction factor with $\Delta\phi < |0.015|$. The reasons, therefore, are the exclusively low impacts of the associated convective heat transfer coefficients on the effective thermal conduction resistance, and this only at configurations with high thermal conductivities of the PCM ($Bi^* \rightarrow 0$).

The results shown in Figure 3 are independent of the selected PCM media, boundary and initial conditions. This can be explained by the fact that the material-specific relationship between enthalpy and temperature does not influence the total heat transport and, thus, the effective thermal conduction resistance or the correction factor ϕ.

Based on the presented results, the correction factor was parameterized as a function of the central dimensionless parameters (Fo, Ψ). For that, a symmetrical sigmoidal approach was used, whose correlation parameters were determined by the results from Figure 3 according to Equation (27).

$$\phi = 0.19(1-\psi)\left(1 - \frac{1}{1 - \frac{Fo}{0.0345\ log(\psi)}}\right) \tag{27}$$

Compared to the simulation data, the correlation shows average and maximum deviations of 1.2% and 16% respectively. The increased deviations occur, in particular, at very low Fourier numbers.

Exemplary results for transient (ξ) characteristics with water as the PCM are shown in Figure 4. A homogeneous starting temperature of 20 °C was assumed for the storage and a cooling temperature of −20 °C for the fluid medium.

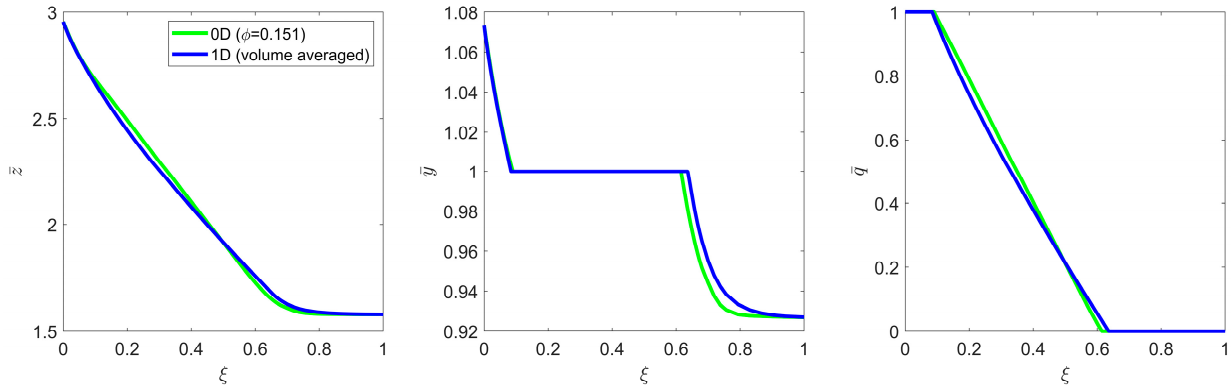

Figure 4. Exemplary comparison between the (1D) substitute model and the 0D-based model for Bi^* = 2, Fo = 16 and Ψ = 0.2: transient results for dimensionless enthalpy $\bar{z}$ (**a**), temperature $\bar{y}$ (**b**) and liquid–solid fraction $\bar{q}$ (**c**).

The temporal characteristics of the dimensionless enthalpy ($\bar{z}$), temperature ($\bar{y}$) and liquid–solid fraction ($\bar{q}$) show very good agreement between the detailed substitute and the 0D-based model. After approx. 10% of the time, the melting temperature at $\bar{y}$ = 1 is reached and the solidification process begins. At the end of the phase change at $\bar{q}$ = 0, there is a further sensible temperature drop down to the cooling temperature.

A verification or validation of the parameterized correction factor (ϕ) as an input variable in the effective heat transfer coefficient ($\bar{k}$) and thus in the dimensionless parameters of the axial model is conducted below using published data on a tube and plate geometry.

4.2. Verification and Validation of the Dimensionless Axial Model

Published data on two latent TES systems, a finned tube [31] and a plate geometry [32], were used to verify and validate the dimensionless axial model according to Equations (9) and (10). The results for the finned tube with salt as the PCM and thermal oil (Syltherm-800) as the heat transfer medium are based on a detailed 2D model, which was additionally verified using CFD simulations. For the plate geometry, experimental results with a wax (RT64HC paraffin) as the PCM and water as the heat transfer medium were used, whereby separate analyses were conducted for charging and discharging.

The required parameters for the axial model were determined based on the respective geometric, material and process-specific values. Firstly, the hydraulic diameters (R_i, R_W and R_a) and the volumetric PCM fraction ($1 - \Psi$) were calculated for each structure. With these equivalent values and with the resulting heat transfer coefficients—for the tube and plate geometry according to [33] and [34]—the dimensionless parameters (Fo, Bi^*) and the correction factors (ϕ) were derived as given in Equation (27). Finally, the effective heat transfer coefficients ($\bar{k}$) for each structure were determined using Equation (23), leading to the required parameters (Π and Λ) for the axial model.

It should be noted here that the central Equations (9) and (24) show identical contexts with different expressions. The dimensionless parameters can therefore also be expressed as a function of each other according to Equation (28).

$$\Pi = 2\frac{\sqrt{\psi}}{1-\psi} Fo \frac{Bi^*}{1 + Bi^* \phi} \tag{28}$$

The dimensionless parameters resulting from the published data for a finned tube (Design A) and plate geometry (Design B) are summarized in Table 2, including the respective initial and boundary conditions.

Table 2. Dimensionless parameters and boundary conditions for model verification and validation.

		Design A [1]	**Design B** [2]	
			Charging	**Discharging**
Dimensionless Parameters	Ψ	0.041	0.696	0.696
	Fo	229.8	0.603	0.201
	ϕ	0.182	0.057	0.056
	Bi^*	0.281	86.7	86.7
	Π	25.98	48.2	16.3
	Λ	0.164	0.151	0.153
Initial Condition	T_{ini} [°C]	172	29	75
Boundary Condition	$T_{F,in,ch}$ [°C]	272	78	
	$T_{F,in,dis}$ [°C]	172		20

[1] Geometric configuration: "plate-1Ph" [31]. [2] Geometric configuration: "Geometry 1" [32].

The central characteristics resulting from this are shown in comparison to the published data for Design A in Figure 5 and for Design B in Figure 6. Information on the respective literature references can be found both in Table 2 and in the Figures 5 and 6. Adiabatic boundary conditions were used for the respective solid media in the axial model, while constant inlet temperatures were used for the fluid media.

In comparison to the detailed CFD- and 2D-based simulation results for Design A (Figure 5), very good agreements were achieved in the heat flow rate between the solid and fluid medium ($\dot{Q}_W$), in the melting and solidification process ($\bar{q}$) and in the outlet temperatures ($T_{F,out}$). Despite the simplifications in the axial model, the relevant transient characteristics were captured in high quality, with differences arising primarily in the area of the constant melting temperature during the phase change.

In contrast, Design B (Figure 6) shows visibly higher deviations with regard to the experimental temperatures T_1 and T_3, although both measuring points themselves show differences despite the same axial location. The reasons for this are not considered to be heat losses in the axial model and in the small test rig configuration with only two plates with associated high boundary effects. Especially for the test rig, a 2D simulation model is formulated in this publication showing, in comparison, higher deviations also during the solidification process ($\bar{q}$), whereby the period of the phase change is in good agreement with the axial model.

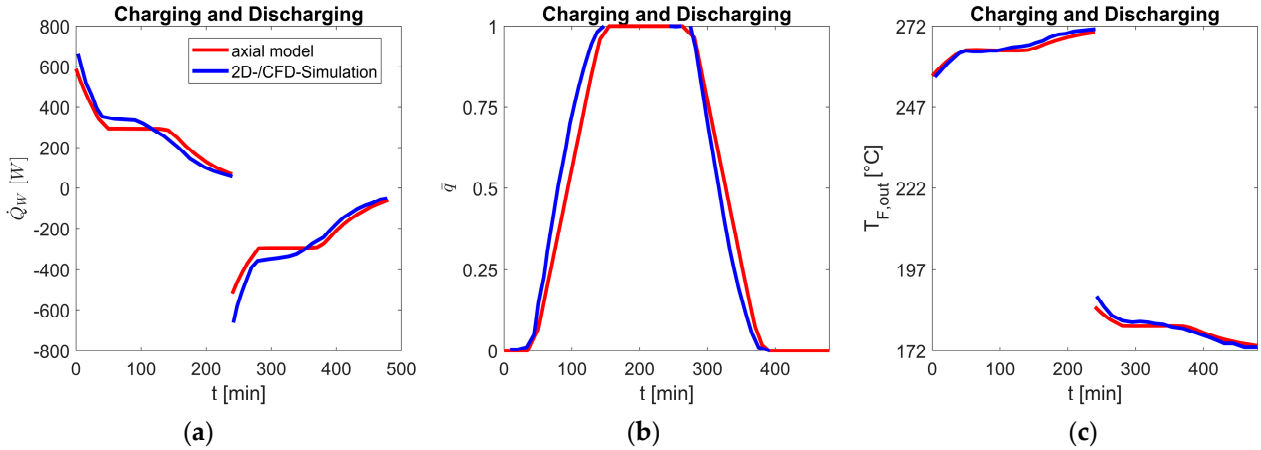

Figure 5. Comparison between 2D-/CFD-based results in Figure 19 of Ref. [31] and the dimensionless axial model: overall heat transfer rate $\dot{Q}_W$ between the solid and fluid medium (**a**), (volume-averaged) melting and solidification process $\bar{q}$ (**b**), outlet temperatures $T_{F,out}$ (**c**).

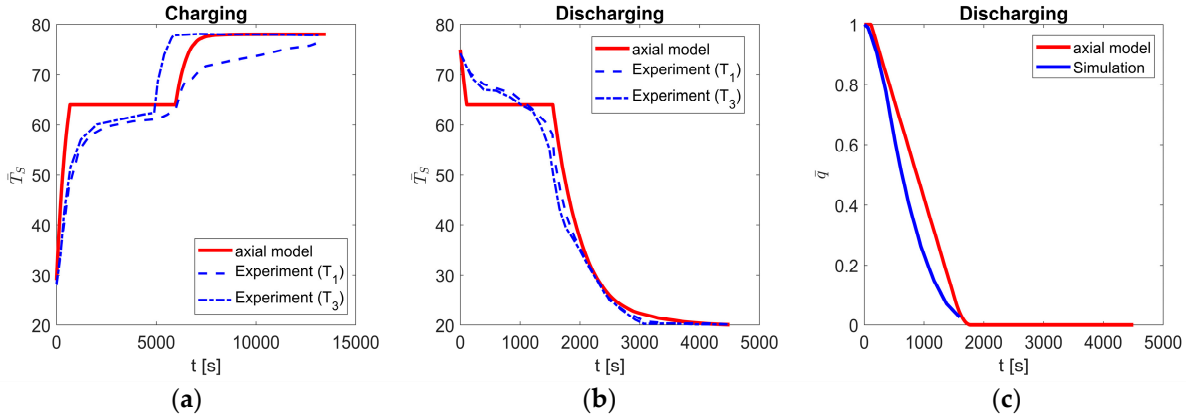

Figure 6. Comparison between experimental/simulative results in Figures 8a, 9a and 11 of Ref. [32] and the dimensionless axial model: local PCM temperature $\overline{T}_S$ for charging (**a**) and discharging (**b**), (volume-averaged) solidification process $\bar{q}$ (**c**).

Despite slight to moderate deviations, the dimensionless axial model confirms an overall good agreement with the relevant transient characteristics of latent TES systems. Significantly different heat-transferring structures, PCMs and process specifications can be captured by the dimensionless parameters, enabling time-efficient design studies. Based on the successfully verified and validated design tool, variation studies are conducted in the following to identify efficient geometric structures in latent TES systems for the cooling supply of BEVs.

4.3. Design Studies: Latent TES Systems for Cold Supply in BEVs

The use of TES systems for BEV air conditioning requires solutions with high storage densities in order to enable integration into the vehicle structure in terms of compactness. But, the low temperature potential between the environment and the storage unit poses significantly higher challenges for cooling demand during warm periods. Solutions with high material-specific storage capacities and effective heat transport between the storage medium and the cold transport medium are necessary to overcome such limitations. The former requirement can be solved with water as a PCM due to its high fusion enthalpy, suitable melting temperature and cost-effective and risk-free handling; the latter can be solved by selecting a suitable heat transfer structure. In addition to water, alternative

materials were also investigated for mobile applications [15] but showed lower values in terms of fusion enthalpy.

4.3.1. Dimensionless Results

In order to identify efficient structures, the dimensionless parameters in the axial model were varied to investigate the thermal performance and cooling efficiency. Detached from the integration concept in the vehicle, cooling temperatures of −10 °C were presupposed for charging the latent TES system, which are in an upper range of potential cooling sources. A systemic elaboration of integration concepts was not considered within the scope of this publication, but is the focus of ongoing R&D activities. The central specifications and target values to identify suitable dimensionless parameters and, thus, heat transfer structures are summarized in Table 3.

Table 3. Specifications of latent TES systems for cooling demands in BEVs during discharge.

T_{ini} [°C]	$T_{F,in}$ [°C]	$T_{F,out,end}$ [°C]	τ [min]	$\dot{Q}_F$ [kW]	Δp [mbar]	p [bar]	PCM	HTF
−10	40	39	30	1	20	1	Water	Air

It was assumed that the latent TES system was cooled homogeneously to −10 °C at the end of the charging period. When driving under extreme summer conditions, the storage unit is discharged at 40 °C until the outlet temperatures reach 39 °C. In line with typical specifications for the heat demand in cold seasons [6], a discharging period of 30 min and a thermal power of 1 kW were applied, whereby the storage system itself may have maximum pressure losses of 20 mbar. Dry air was used as the heat transfer medium to discharge the storage system.

Based on these typical specifications, iterative variation studies were performed on the dimensionless parameters Π and Λ in the axial model (Equations (9) and (10)) in order to fulfil the defined target value ($T_{F,out,end}$). The results are shown in Figure 7.

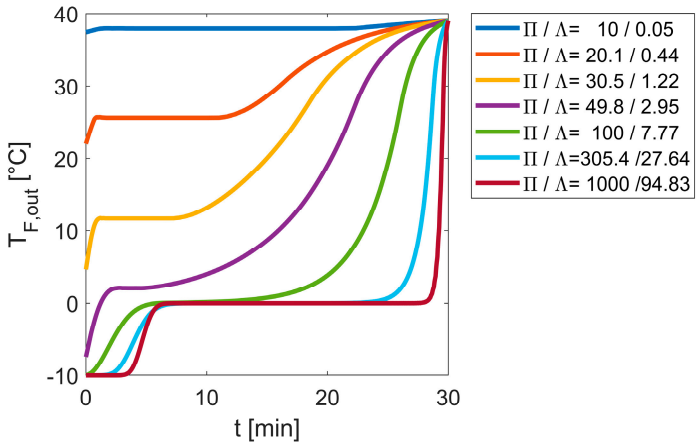

Figure 7. Fluid outlet temperatures during discharge as a function of the dimensionless parameters Π and Λ in the axial model.

The transient characteristics show that the specified outlet temperature of 39 °C is reached at the end of the discharge period for the iteratively determined solutions. With increasing dimensionless parameters, lower (temporally averaged) outlet temperatures result, thus resulting in higher efficiencies. The reason for this behavior is associated with the heat-transferring structures—expressed in a dimensionless way through parameters Π and Λ—achieving high heat transfer between the storage and fluid medium through high specific surfaces and effective transfer coefficients.

Resulting from Figure 7, the discharge duration and thermal power as specified in Table 3 and the expressions in Equations (11) and (12), the respective mass flow rates and storage masses (water) can be determined on the basis of (integrally) averaged outlet temperatures. Together with geometry-dependent correlations to heat transfer coefficients and pressure losses for the considered structures (tubes [35], finned plates [36], TPMS–Fischer-Koch S [28]), these results serve as input data for an iterative determination of the two central equivalent values via Equations (23) and (27): the hydraulic diameter (R_W) or the specific surface (a_W) and the volumetric PCM fraction ($1 - \Psi$). Design-specific results for the evaluation and selection of favored structures are presented below.

4.3.2. Case Study for Latent TES with High Storage Density: Tube vs. Finned Plate vs. TPMS

For the identification of effective heat-transferring structures in latent TES systems for the cooling supply of BEVs, tube, finned plate and TPMS geometries (Fischer-Koch S) were investigated using the presented dimensionless methodology. To reduce the solution space and to enforce geometrically comparable solutions in addition to the uniform thermal and pressure loss conditions (Table 3), additional (geometric) specifications were defined: the length-to-diameter ratio (L/D) in the range of 0.5–4, the heat-transferring wall thickness (1 mm, aluminum) and, specifically for the plate structure, the fin height and length in the range of 1–100 mm. Within this range and with the given dimensionless values (Π and Λ) from Section 4.3.1, designs were iteratively determined through the two equivalent values (a_W, Ψ).

The results for gravimetric storage densities and one equivalent value (a_W) as a function of the (integrally) averaged outlet temperatures ($\overline{T}_{F,out}$) are shown in Figure 8. It should be noted that the gravimetric storage density includes the total mass (m_{tot}) of the PCM (water), heat-transferring geometry and enclosure.

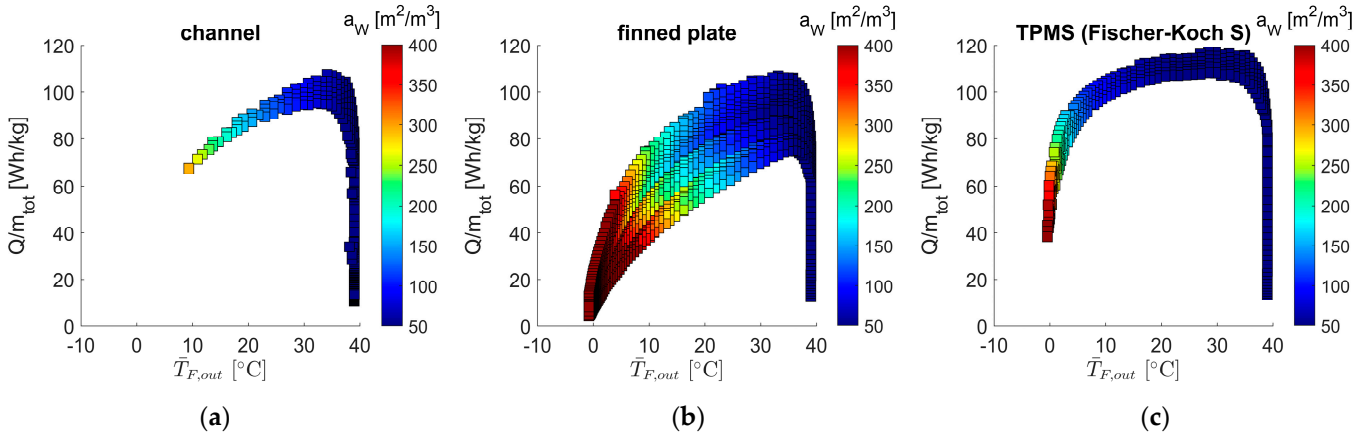

Figure 8. Gravimetric storage densities as a function of (integrally) averaged outlet temperatures ($\overline{T}_{F,out}$) and specific surfaces (a_W) for channel (**a**), finned plate (**b**) and TPMS (**c**) design options.

Regardless of the considered structure, the results show decreasing gravimetric storage densities at high or low (integrally) averaged outlet temperatures. The reasons for this are increasing PCM masses in design solutions with low specific surfaces and, thus, poor efficiencies, as well as a significant increase in the weight of the heat-transferring wall in design solutions with high specific surfaces. Together with the uniform L/D ratio, cooling capacity and pressure loss, only limited results up to approx. 10 °C are visible with tube structures compared to plate or TPMS structures due to their comparatively lower heat transfer effectiveness. The most effective heat transport with the lowest mass under the same boundary conditions is reached by TPMS structures. Such potentials have also been shown for TMPS options in conventional heat exchanger applications [37].

The results for the second iteratively determined equivalence value—volumetric fraction of the PCM ($1 - \Psi$)—pointed out for all considered structures that increasing

gravimetric storage densities are accompanied by low space requirements on the fluid side. Here, an upper limit is given by the heat-transferring structure and its wall thickness.

Based on these results from Figure 8 and for an exemplary defined requirement—cooling the warm air to an (integrally) averaged outlet temperature ($\overline{T}_{F,out}$) of 10 °C—the central design-specific values for the latent TES systems are summarized in Table 4 as a basis for evaluation. In each case, solutions with the highest gravimetric storage densities were selected.

Table 4. Gravimetric and volumetric storage densities of latent TES systems for cooling demands in BEVs and central geometric specifications of the identified design options.

Design	Q/m_{tot} [Wh/kg]	Q/V_{tot} [kWh/m³]	a_W [m²/m³]	$1-\Psi$ [%]	L/D
Tube	71.4	90.3	264	66	4
Finned Plate (OSF)	76.7	89.3	214	64	1
TPMS (Fischer-Koch S)	102.2	100	83	73	3

In comparison, the advantages of TPMS-based structures in terms of gravimetric and volumetric storage density with only moderately high required specific surfaces are obvious. Here, only in relation to the PCM—without wall structures, internal fluid paths and the enclosure—can approx. 69% of the maximum possible storage density be utilized, whereby additional capacitive terms—the TPMS structure itself—were not considered. Alternative solutions are offered by finned plates with commercially available specific surfaces. Tube geometries, however, achieve comparable dimensions, but with untypical high specific surfaces and, thus, very small hydraulic diameters of 5 mm. The technical feasibility can therefore be seen as critical due to the large number of required pipes.

The identified TPMS structure for this application using the presented top-down methodology and the dimensionless model with associated time-relevant characteristics is shown in Figure 9.

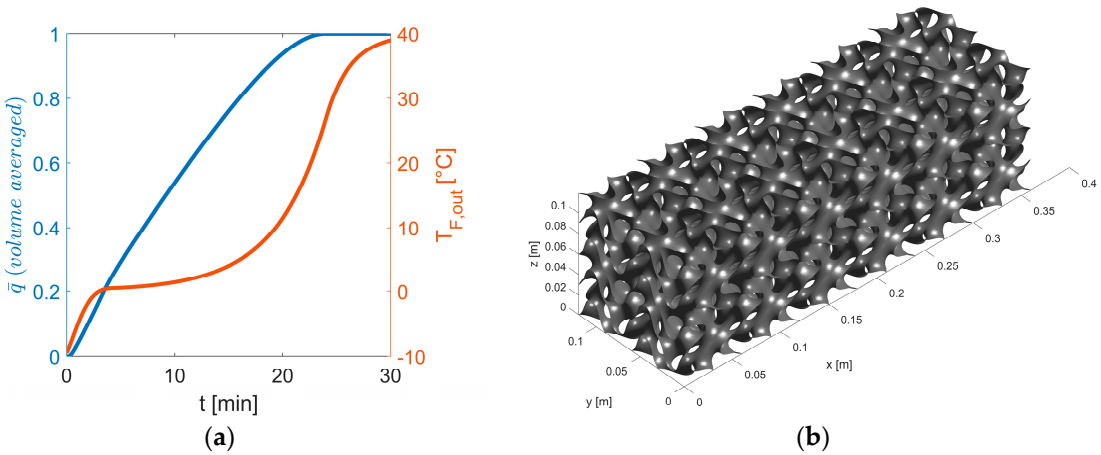

Figure 9. Fluid outlet temperature ($T_{F,out}$) and (volume-averaged) melting process $\bar{q}$ during discharging (**a**) of the identified TPMS structure (**b**).

The transient results show that a complete melting of the PCM (water) is achieved after approx. 23 min and that the specified outlet temperature of 39 °C is reached by the end of the discharge. The TPMS structure required for this has a length of 36 cm and a square cross-section of 12 cm with Fischer-Koch S cell sizes of 6 cm. In addition to aluminum as the material for the heat-transferring structure, variation studies were also conducted with a plastic option (PEEK). Despite the lower heat conduction in the plastic structure, slightly

higher storage densities were found compared to those with aluminum. The reasons for this are the lower density of PEEK and the remaining dominant thermal conduction resistance in the PCM.

The identified TPMS structure confirms that high storage densities of latent TES systems are reachable for cooling demands in BEVs. However, further development of this efficiency-enhancing solution will require investigations into integration and charging options inside the BEV system as well as detailed analyses of heat losses and dynamic operation management. However, the identified design provides a successful starting point for this.

5. Conclusions

In stationary applications, TES systems enable flexible options for further expansion of renewable energies due to their time-decoupled operation. Transferring this technology to BEVs aims to increase their range by providing alternative air conditioning while driving, whereby so far only heat has been focused on. Solutions for efficient and compact TES systems for cooling requirements during warm seasons are missing but are necessary to enable efficient thermal management concepts over the whole year.

Detached from the charging procedure, design solutions with high storage densities are needed in order to fulfill space requirements in the vehicle. For the heat demand, this is achieved through a TES system with high temperatures; for the cooling—due to the significantly lower temperature potentials—this is achieved through a latent TES system with water as the PCM, but requires an effective (internal) heat-transferring structure. However, the identification of such a structure is associated with high conceptual and simulation efforts due to the large number of geometric options. To overcome this hurdle, a top-down methodology with a dimensionless model for latent TES systems was presented, which allows for transient analyses and the time-efficient derivation of suitable structures based on just a few parameters.

Therefore, an axial enthalpy and temperature-based model was de-dimensionalized using normalization and relation procedures, whereby the thermal conduction resistance within the PCM is captured by a dimensionless parameterization. The systematically derived model is based on geometric equivalence values and was successfully verified and validated using published data on two different structures. Subsequently, the design tool served as a basis for identifying efficient structures in water–ice-based latent TES systems for cooling supply in BEVs. A wide array of variation studies on tube, finned plate geometries and novel TPMS structures were performed with the application of typical boundary conditions and were uniformly evaluated with regard to storage densities, cooling efficiencies and geometric requirements. The results show that high gravimetric and volumetric storage densities including the enclosure of 100 Wh/kg or 102.2 kWh/m^3 at average cooling capacities of 1 kW over 30 min can be achieved for TPMS structures (Fischer-Koch S). The identified TPMS structure itself has a length of 36 cm, a square cross-section of 12 cm and Fischer-Koch S cell sizes of 6 cm. Further slight improvements can be reached by choosing plastic (PEEK) instead of aluminum as the material for the heat-transferring structure.

The identified solution using the presented methodology and dimensionless model confirms that high storage densities of latent TES systems are feasible for cooling requirements in BEVs, reaching comparable effectiveness to TES options for heating demands. Further development of this efficiency-enhancing solution will require investigations into integration and charging options as well as into heat loss and dynamic operation management.

Author Contributions: Methodology, V.D; validation, V.D.; formal analysis, V.D.; investigation, V.D.; writing—original draft preparation, V.D.; supervision, A.G. All authors have read and agreed to the published version of the manuscript.

Funding: This research received no external funding.

Data Availability Statement: The original contributions presented in this study are included in the article. Further inquiries can be directed to the corresponding author.

Conflicts of Interest: The authors declare no conflicts of interest.

References

1. Paul, A.; Holy, F.; Textor, M.; Lechner, S. High temperature sensible thermal energy storage as a crucial element of Carnot Batteries: Overall classification and technical review based on parameters and key figures. *J. Energy Storage* **2022**, *56*, 106015. [CrossRef]
2. Alami, K.E.; Asbik, M.; Agalit, H. Identification of natural rocks as storage materials in thermal energy storage (TES) system of concentrated solar power (CSP) plants—A review. *Sol. Energy Mater. Sol. Cells* **2020**, *217*, 110599. [CrossRef]
3. Budt, M.; Wolf, D.; Span, R.; Yan, J. A review on compressed air energy storage: Basic principles, past milestones and recent developments. *Appl. Energy* **2016**, *170*, 250–268. [CrossRef]
4. Krüger, M. Systematic Concept Study of Brayton Batteries for Coupled Generation of Electricity, Heat, and Cooling. *Appl. Sci.* **2024**, *14*, 6073. [CrossRef]
5. Belik, S.; Dreißigacker, V.; Zunft, S. Power-to-heat integration in regenerator storage: Enhancing thermal storage capacity and performance. *J. Energy Storage* **2022**, *50*, 104570. [CrossRef]
6. Kuper, C.; Hoh, M.; Houchin, G.-M.; Fuhr, J. *Thermal Management of Hybrid Vehicle Battery Systems*; EVS24: Stavanger, Norway, 2009.
7. Dieterich, M.; Bürger, I.; Linder, M. Open and closed metal hydride system for high thermal power applications: Preheating vehicle components. *Int. J. Hydrogen Energy* **2017**, *42*, 11469–11481. [CrossRef]
8. Melnik, D.; Bürger, I.; Mitzel, J.; Käß, J.; Sarkezi-Selsky, P.; Jahnke, T.; Knöri, T. Energy efficient cold start of a Polymer Electrolyte Membrane Fuel Cell coupled to a thermochemical metal hydride preheater. *Appl. Energy* **2024**, *359*, 122585. [CrossRef]
9. Dreißigacker, V. Solid Media Thermal Energy Storage System for Heating Electric Vehicles: Advanced Concept for Highest Thermal Storage Densities. *Appl. Sci.* **2020**, *10*, 8027. [CrossRef]
10. Kraft, W.; Stahl, V.; Vetter, P. Thermal Storage Using Metallic Phase Change Materials for Bus—State of the Art of Electric Buses and Requirements for the Storage System. *Energies* **2020**, *13*, 3023. [CrossRef]
11. Luo, C.; Xie, P.; Chen, G.; Mao, L.; Liu, L.; Jin, L.; Cheng, Z.; Xu, J.; Qiao, G. Prototype design and experimental study of a metal alloy-based thermal energy storage system for heat supply in electric vehicles. *J. Energy Storage* **2022**, *51*, 104393. [CrossRef]
12. Dreißigacker, V.; Hofer, L. High-Performance Solid Medium Thermal Energy Storage System for Heat Supply in Battery Electric Vehicles: Proof of Concept and Experimental Testing. *Appl. Sci.* **2022**, *12*, 943. [CrossRef]
13. Ugurlu, A.; Gokcol, C. A review on thermal energy storage systems with phase change materials in vehicles. *Electron. J. Vocat. Coll.* **2012**, *2*, 251–283.
14. Li, C.; Peng, M.; Xie, B.; Li, Y.; Li, M. Novel phase change cold energy storage materials for refrigerated transportation of fruits. *Renew. Energy* **2024**, *220*, 119583. [CrossRef]
15. Yenare, R.R.; Sonawane, C.R.; Sur, A.; Singh, B.; Panchal, H.; Kumar, A.; Sadasivuni, K.K.; Siddiqui, M.I.H.; Bhalerao, Y. A comprehensive review of portable cold storage: Technologies, applications, and future trends. *Alex. Eng. J.* **2024**, *94*, 23–33. [CrossRef]
16. Zhang, Y.; Yang, X.; Zou, S.; Xu, X.; Tu, Y.; Tian, Y.; Ke, Z. Enhancing the phase change material based shell-tube thermal energy storage units with unique hybrid fins. *Int. Commun. Heat Mass Transf.* **2024**, *157*, 107763. [CrossRef]
17. Gürel, B. A numerical investigation of the melting heat transfer characteristics of phase change materials in different plate heat exchanger (latent heat thermal energy storage) systems. *Int. J. Heat Mass Transf.* **2020**, *148*, 119117. [CrossRef]
18. Iyer, J.; Moore, T.; Nguyen, D.; Roy, P.; Stolaroff, J. Heat transfer and pressure drop characteristics of heat exchangers based on triply periodic minimal and periodic nodal surfaces. *Appl. Therm. Eng.* **2022**, *209*, 118192. [CrossRef]
19. Kim, J.; Yoo, D.-J. 3D printed compact heat exchangers with mathematically defined core structures. *J. Comput. Des. Eng.* **2020**, *7*, 527–550. [CrossRef]
20. Fan, Z.; Fu, Y.; Gao, R.; Liu, S. Investigation on heat transfer enhancement of phase change material for battery thermal energy storage system based on composite triply periodic minimal surface. *J. Energy Storage* **2023**, *57*, 106222. [CrossRef]
21. Qureshi, Z.A.; Elnajjar, E.; Al-Ketan, O.; Al-Rub, R.A.; Al-Omari, S.B. Heat transfer performance of a finned metal foam-phase change material (FMF-PCM) system incorporating triply periodic minimal surfaces (TPMS). *Int. J. Heat Mass Transf.* **2021**, *170*, 121001. [CrossRef]
22. Lee, A.H.W.; Jones, J.W. Modeling of an ice-on-coil thermal energy storage system. *Energy Convers. Manag.* **1996**, *37*, 1493–1507. [CrossRef]
23. Toffoletti, G.; Cortella, G.; D'Agaro, P. Thermodynamic and economic seasonal analysis of a transcritical CO_2 supermarket with HVAC supply through ice thermal energy storage (ITES). *J. Clean. Prod.* **2024**, *434*, 139832. [CrossRef]
24. London, A.L.; Seban, R.A. Rate of Ice Formation. *ASME. Trans.* **1943**, *65*, 771–778. [CrossRef]
25. Schmidt, F.W.; Willmott, A.J. *Thermal Energy Storage and Regeneration*; McGraw-Hill Book Company: New York, NY, USA, 1981.
26. Ismail, K.A.R.; Stuginsky, R. A parametric study on possible fixed bed models for pcm and sensible heat storage. *Appl. Therm. Eng.* **1999**, *19*, 757–788. [CrossRef]
27. Kuznik, F.; Lopez, J.P.A.; Baillis, D.; Johannes, K. Design of a PCM to air heat exchanger using dimensionless analysis: Application to electricity peak shaving in buildings. *Energy Build.* **2015**, *106*, 65–73. [CrossRef]

28. Wang, J.; Chen, K.; Zeng, M.; Ma, T.; Wang, Q.; Cheng, Z. Investigation on flow and heat transfer in various channels based on triply periodic minimal surfaces (TPMS). *Energy Convers. Manag.* **2023**, *283*, 116955. [CrossRef]
29. Brambati, G.; Guilizzoni, M.; Foletti, S. Convective heat transfer correlations for Triply Periodic Minimal Surfaces based heat exchangers. *Appl. Therm. Eng.* **2024**, *242*, 122492. [CrossRef]
30. Schumann, T.E.W. Heat transfer: A liquid flowing through a porous prism. *J. Frankl. Inst.* **1929**, *208*, 405–416. [CrossRef]
31. Vogel, J.; Keller, M.; Johnson, M. Numerical modeling of large-scale finned tube latent thermal energy storage systems. *J. Energy Storage* **2020**, *29*, 405–416. [CrossRef]
32. Taghavi, M.; Poikelispää, M.; Agrawal, V.; Syrjälä, S.; Joronen, T. Numerical investigation of a plate heat exchanger thermal energy storage system with phase change material. *J. Energy Storage* **2023**, *61*, 106785. [CrossRef]
33. Winterton, R.H.S. Where did the Dittus and Boelter equation come from? *Int. J. Heat Mass Transf.* **1998**, *41*, 809–810. [CrossRef]
34. Wang, C.-C.; Lee, C.-J.; Chang, C.-T.; Lin, S.-P. Heat transfer and friction correlation for compact louvered fin-and-tube heat exchangers. *Int. J. Heat Mass Transf.* **1998**, *42*, 1945–1956. [CrossRef]
35. Kakaç, S.; Shah, R.K.; Aung, W. *Handbook of Single-Phase Convective Heat Transfer*; Wiley: New York, NY, USA, 1987.
36. Manglik, R.M.; Bergles, A.E. Heat transfer and pressure drop correlations for the rectangular offset strip fin compact heat exchanger. *Exp. Therm. Fluid Sci.* **1995**, *10*, 171–180. [CrossRef]
37. Knödler, P.; Dreissigacker, V. Fluid Dynamic Assessment and Development of Nusselt Correlations for Fischer Koch S Structures. *Energies* **2024**, *17*, 688. [CrossRef]